Allosteric Inhibition of HER2 by Moesin-Mimicking Compounds Targets HER2-Positive Cancers and Brain Metastases

Camille Faure[1], Rym Djerbi-Bouillié[1], Anaïs Domingot[1], Haniaa Bouzinba-Segard[1], Saïd Taouji[2], Yanis Saidi[1], Sandra Bernard[1], Floriane Carallis[1], Romy Rothe-Walther[3], Jean-Luc Lenormand[3], Eric Chevet[2], and Sandrine Bourdoulous[1]

ABSTRACT

Therapies targeting the tyrosine kinase receptor HER2 have significantly improved survival of patients with HER2$^+$ cancer. However, both *de novo* and acquired resistance remain a challenge, particularly in the brain metastatic setting. Here we report that, unlike other HER tyrosine kinase receptors, HER2 possesses a binding motif in its cytosolic juxtamembrane region that allows interaction with members of the Ezrin/Radixin/Moesin (ERM) family. Under physiologic conditions, this interaction controls the localization of HER2 in ERM-enriched domains and stabilizes HER2 in a catalytically repressed state. In HER2$^+$ breast cancers, low expression of Moesin correlated with increased HER2 expression. Restoring expression of ERM proteins in HER2$^+$ breast cancer cells was sufficient to revert HER2 activation and inhibit HER2-dependent proliferation. A high-throughput assay recapitulating the HER2–ERM interaction allowed for screening of about 1,500 approved drugs. From this screen, we found Zuclopenthixol, an antipsychotic drug that behaved as a Moesin-mimicking compound, because it directly binds the juxtamembrane region of HER2 and specifically inhibits HER2 activation in HER2$^+$ cancers, as well as activation of oncogenic mutated and truncated forms of HER2. Zuclopenthixol efficiently inhibited HER2$^+$ breast tumor progression *in vitro* and *in vivo* and, more importantly, showed significant activity on HER2$^+$ brain tumor progression. Collectively, these data reveal a novel class of allosteric HER2 inhibitors, increasing the number of approaches to consider for intervention on HER2$^+$ breast cancers and brain metastases.

Significance: This study demonstrates the functional role of Moesin in maintaining HER2 in a catalytically repressed state and provides novel therapeutic approaches targeting HER2$^+$ breast cancers and brain metastasis using Moesin-mimicking compounds.

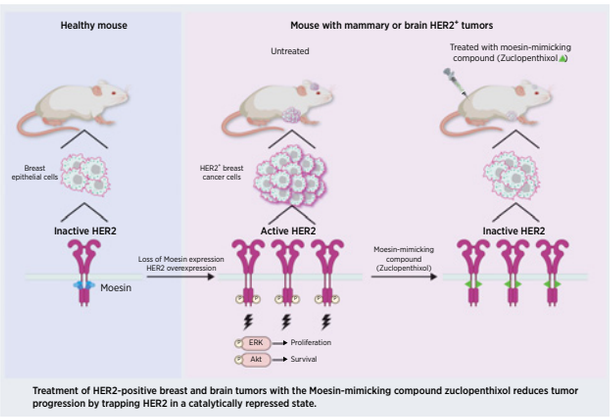

Treatment of HER2-positive breast and brain tumors with the Moesin-mimicking compound zuclopenthixol reduces tumor progression by trapping HER2 in a catalytically repressed state.

Introduction

HER2$^+$ breast cancer is defined by amplification of the ERBB2/HER2/Neu oncogene and/or overexpression of its associated HER2 transmembrane receptor protein (1). HER2$^+$ breast tumors represent approximately 20% to 25% of breast cancers and are associated with a higher grade, more aggressive phenotype, and worse prognosis. With the advent of antibody-based (trastuzumab, pertuzumab) or small-molecule tyrosine kinase inhibitors (lapatinib) targeting HER2, the prognostic landscape for patients with HER2$^+$ breast cancer has considerably improved (2). However, both *de novo* and acquired resistance to trastuzumab and cardiotoxic side effects of these inhibitors remain a significant obstacle for extensive use of these treatments (3). About 30% of HER2$^+$ breast tumors express a truncated form of HER2 (p95HER2), which confers resistance to trastuzumab and is associated with worse outcome in trastuzumab-treated patients (4, 5). More recently, somatic *HER2* gene mutations were detected in a range of human cancer types that functionally activate HER2, drive and maintain cancers, and that can also confer resistance to HER2-directed drugs (6). Finally, these targeted therapies have limited ability to cross the blood–brain barrier (BBB) and show low efficacy against brain lesions. Brain metastasis, occurring in up to 50% of the trastuzumab-treated patients, is an end in breast cancer progression (7), requiring novel therapies for successful treatment.

HER2 is a member of the HER family (EGFR/HER1, HER2, HER3, HER4) of transmembrane receptor tyrosine kinases (RTK) involved in various cellular processes including cell proliferation, motility, resistance to apoptosis, invasiveness, and angiogenesis. This RTK displays unique properties. Structurally, HER2 contains an extracellular domain (amino-acids 1–639) locked in an open conformation, a

[1]Université de Paris, Institut Cochin, Inserm, CNRS, Paris, France. [2]Inserm, Université de Bordeaux, Institut Bergonié, Bordeaux, France. [3]TIMC-IMAG Laboratory, CNRS, Université Joseph Fourier, UFR de Médecine, La Tronche, France.

Note: Supplementary data for this article are available at Cancer Research Online (http://cancerres.aacrjournals.org/).

Corresponding Authors: Sandrine Bourdoulous, Institut Cochin, 22 rue Méchain, Paris 75014, France. Phone: 331-4051-6427; E-mail: sandrine.bourdoulous@inserm.fr; and Camille Faure, camille.faure@inserm.fr

Cancer Res 2021;81:5464–76

doi: 10.1158/0008-5472.CAN-21-0162

hydrophobic transmembrane domain (aa 640–672), a cytosolic juxtamembrane region (673–701), a tyrosine kinase domain (aa 720–977), and a C-terminal tail with regulatory tyrosine residues (978–1255; refs. 8–10). A critical distinction defining its unique cell-signaling mode is its ability to promote its ligand-independent autodimerization and phosphorylation (11), as well as ligand-dependent heterodimerization and phosphorylation with the other HER family members (10, 12). In $HER2^+$ breast cancers, HER2/HER3 heterodimerization promotes HER2 phosphorylation and phosphorylation of the kinase defective HER3, leading to stimulation of the downstream oncogenic PI3K/AKT pathway, while HER2 homodimerization leads to downstream oncogenic RAS–MAPK and indirect PI3K–AKT pathway activation (11, 13, 14).

Ezrin, Radixin, Moesin (ERM) proteins are involved in many cellular processes (15). These cytosolic proteins localize at cell surface–associated structures, such as microvilli and cell-adhesion sites (16). They link transmembrane proteins and the cortical cytoskeleton by interacting with a RxxTYxVxxA motif located in the juxtamembrane region of several adhesion molecules, such as the hyaluronic receptor CD44, through their N-terminal FERM domain and by interacting through their C-terminal domain with F-actin (17–19). They are critical players in cell migration, growth, and adhesion, but also cell invasion and metastasis formation (15, 16).

Here, we found that HER2 possesses a binding motif in its intracellular juxtamembrane region allowing allosteric inhibition by members of the ERM family. In $HER2^+$ breast cancers, low Moesin expression correlates with increased HER2 expression. Through a high-content screen designed to identify Moesin-mimicking compounds, we discovered Zuclopenthixol. This compound efficiently inhibited activation of oncogenic forms of HER2, and specifically blocked $HER2^+$ breast cancer progression both *in vitro* and *in vivo*. Finally, known to cross the blood–brain barrier, it attenuated the growth of $HER2^+$ breast tumors following brain implantation. These findings reveal a novel class of allosteric HER2 inhibitors with activity on both breast- and brain-localized tumors, which could markedly improve the treatment of $HER2^+$ breast cancer and metastases.

Materials and Methods

Reagents

A list of the antibodies used in this work is provided in Supplementary Table S1.

Zuclopenthixol hydrochloride, Flupenthixol, and derived analogues were synthetized and purified by Roowin.

Plasmids and mutagenesis

The list of primers and siRNA used in this work is provided in Supplementary Table S2. The vectors used in this work are detailed in the Supplementary Materials and Methods.

Cell culture and transfection

Human bone marrow endothelial cells (HBMEC) kindly provided by Dr. B. Weksler (Weill Medical College of Cornell University, New York, NY) and Caco-2/TC7 cells kindly provided by Dr. M. Rousset (Université Pierre et Marie Curie, Paris, France) were cultured as described previously (20, 21). The porcine kidney epithelial cell line, LLC-PK1, the human breast cancer cell lines (SKBR3, BT474, MDA-MB-231, and HCC1954) were obtained from the ATCC and were maintained in DMEM or RPMI1640 (HCC1954) containing 10% FBS. All cell lines were cultured under 5% CO_2 at 37°C. HBMECs and LLC-PK1 were transfected using Amaxa Inc nucleofector system (Kit V and U015 program) or Bio-Rad electroporation system, respectively, as described previously (22, 23). SKBR3, BT474, and HCC1954 were transfected with Amaxa using Kit C and E009 program. Proliferation and soft-agar colony formation assays are described in Supplementary Methods. Periodic tests for *Mycoplasma* and authentication were performed using commercially available kits.

Transcriptomic analyses

HER2 and Moesin mRNA expression levels in patients with breast-invasive carcinoma ($n = 526$), stomach adenocarcinoma ($n = 478$), bladder urothelial carcinoma ($n = 408$), pancreatic adenocarcinoma ($n = 178$), colorectal adenocarcinoma ($n = 379$), ovarian serous cystadenocarcinoma ($n = 304$), kidney renal clear cell carcinoma ($n = 533$), and kidney renal papillary cell carcinoma ($n = 290$) were from The Cancer Genome Atlas (TCGA), Firehose Legacy. HER2 and Moesin mRNA levels in patients with cervical squamous cell carcinoma ($n = 278$) were from TCGA, PanCancer Atlas. mRNA data were z-scores relative to diploid samples (RNA Seq V2 RSEM) downloaded through cBioPortal (http://www.cbioportal.org). Cancer cell lines mRNA expression data were obtained from E-MTAB-2706 study (https://www.ebi.ac.uk/arrayexpress/).

Breast cancer tissue array

Sections from breast cancer tissue array (FFPE) including IHC results of HER2\ER\PR\Ki67 for 3 normal breast tissue and breast fibroadenoma, 2 breast cystosarcoma phyllodes, 7 breast intraductal carcinoma, and 60 breast-invasive ductal carcinoma, with duplicate cores per case were purchased from US Biomax, Inc (https://www.biomax.us/tissue-arrays/Breast/BR1503f). They were processed for IHC using HER2, Ezrin, or Moesin antibodies using a fully automated Leica BondIII stainer, according to the manufacturer's recommendations. Sections were then lightly counterstained with hematoxylin, dehydrated, and cleared in graded alcohol and Ottix plus (MM-France), and finally covered with glass slips. Samples were scanned using a Lamina multilabel slide scanner (PerkinElmer) and were classified on the basis of visual scoring of Moesin-positive tumor cells as Moesin low (0%–10%), intermediate (11%–50%), or high (>50%) expressing samples.

Tumor progression in orthotopic xenograft model

Experiments were performed on the TrGET platform of Centre de Recherche de Cancérologie de Marseille (Institut Paoli Calmettes, Marseille, France) in accordance with the guidelines of the Institut National de la Santé et de la Recherche Médicale. The experimental protocol was approved by the Animal Experimentation Ethics Committee of Marseille (APAFIS#2079–2015092811101360 v3). Briefly, 5×10^6 BT474 cells resuspended in 100 μL (50% Matrigel and 50% PBS) were implanted orthotopically in the mammary fat pad of NOD.Cg-Prkdc scid/J mice anesthetized with ketamine and xylazine and administered with metacam (s.c., 1 mg/kg). Estradiol pellets were implanted subcutaneously. Metacam was administered 24 and 48 hours postimplantation. Nineteen days postimplantation, mice were randomized into three groups to be administered intraperitoneally during three weeks with vehicle (10% DMSO in PBS, 5 days a week, $n = 9$), 4 mg/kg Zuclopenthixol (5 days a week, $n = 8$), or 5 mg/kg Zuclopenthixol (3 days a week, $n = 9$). Mice weight and tumor volume were assessed two to three times a week using a caliper. At the end of the experiment, the collected tumors were photographed, weighed, cut into halves to be either frozen in liquid nitrogen or embedded in optimal cutting temperature medium, and frozen at −80°C. A tissue

Lyzer was used to solubilize tumor proteins in a buffer containing 50 mmol/L Tris (pH = 8.8), 25 mmol/L NaCl, 1 mmol/L EDTA, 1% Triton, 10% glycerol and 1 mmol/L phosphatase (AEBSF and 1 mmol/L orthovanadate), and 10 μg/mL protease inhibitors (aprotinin, leupeptin, pepstatin). Five-micron–thick sections were immobilized on Superfrost plus microscope slides and processed for immunofluorescence or IHC analyses. Samples were scanned using a Lamina multilabel slide scanner (PerkinElmer) and were further analyzed using confocal microscopy (spinning disk Leica, 40×). For quantitative analysis, fluorescence intensity of Ki67 and DAPI labeling was measured using ImageJ software and the proliferation index was displayed as a ratio between Ki67-stained area over DAPI-stained area.

Tumor progression in intracranial xenograft model

Experiments were performed by Oncodesign contract research organization (Dijon, France). The experimental protocol was approved by the Animal Experimentation Ethics Committee OnCoMet (study: 180078ET100). Briefly, 1×10^5 BT474 cells resuspended in 2 μL RPMI1640 medium were stereotactically implanted into the caudate nucleus of the right cerebral hemisphere of female BALB/c nude mice, 4–5 weeks old, under gas anesthesia with isoflurane. Drinking water was supplemented with estradiol (2.5 μg/mL). In the first set of experiments, MRI was performed at day 10, mice were then randomized and intraperitoneally received Zuclopenthixol ($n = 10$, 7 mg/kg on Monday and Tuesday and 10 mg/kg on Wednesday, Thursday, and Friday) or vehicle ($n = 10$, 20% w/v hydroxypropyl-β-cyclodextrin per day for 5 consecutive days a week) and a second MRI was performed at day 20. In the second set of experiments, implanted mice were randomized at day 3 and intraperitoneally received Zuclopenthixol, vehicle at doses identical to the first set or received lapatinib (100 mg/kg, orally, $n = 10$). MRI scans were performed at days 15 and 26 postimplantation. During MRI, mice were continuously anesthetized using isoflurane. Gadopentetate dimeglumine (Gd-DTPA, Magnevist, Bayer Healthcare Pharmaceuticals) was injected intravenously at 0.4 mmol/kg. MRI scans were acquired on a 4. 7T horizontal magnet (PharmaScan, Bruker Biospin GmbH) equipped with an actively shielded gradient system with the following parameters: time of repetition = 700 ms, echo time = 12 ms, field of view = 40 mm × 40 mm, acquisition matrix = 384 × 384, slice thickness = 0.8 mm, slice gap = 0.8 mm, slice number = 10, and number of averages = 4. The positions of the slices were determined using sagittal, coronal, and axial imaging. MR images were acquired under Para Vision (PV5.1, Bruker Biospin) and analyzed under ImageJ. Regions of interest were drawn manually on anatomic images. Tumor volume was computed from these regions by multiplying the number of voxels by the voxel volume (in mm^3).

Statistical analysis

Statistical analyses were performed by GraphPad Prism 5 software. Unpaired/paired Student t test was used to analyze the statistical difference of two groups. One- or two-way ANOVA test followed by multiple comparison test, as indicated, was used to analyze the statistical difference between multiple groups. The correlation between HER2 and ERM expression was analyzed by Spearman r correlation coefficient. Data are presented as the mean ± SD or SEM as indicated. $P < 0.05$ was considered statistically significant.

Additional Materials and Methods are provided in the Supplementary Information.

Results

ERM proteins Ezrin and Moesin interact with HER2 and address HER2 to ERM-enriched regions

A direct interaction between the FERM domain of the ERM proteins and a R/KxxxYxL/V/IxxA motif located in the cytosolic juxtamembrane regions of intercellular adhesion molecules (ICAM-1,-2, -3) CD43 and CD44 was previously reported (17, 19). We identified in the cytosolic juxtamembrane region of HER2 a similar ERM-binding motif between Lys-676 and Leu-691, which was absent in other EGFR family members (**Fig. 1A**). To address whether this motif also allows interaction of HER2 with the ERM proteins, we generated a glycoprotein D-tagged HER2 form harboring mutations in the critical amino acid residues involved in this ERM-binding motif (gD-HER2-EBM*; **Fig. 1A**). When ectopically expressed in human endothelial cells (HBMEC), the wild-type gD-tagged form of the receptor (gD-HER2-WT) coimmunoprecipitated with Ezrin and Moesin (**Fig. 1B**). Although gD-HER2-EBM* construct was immunoprecipitated to a lower extent, interaction was drastically reduced with this construct (**Fig. 1B**). In addition, both endogenous HER2 (Supplementary Fig. S1A) and gD-HER2-WT (**Fig. 1C**) were efficiently pulled down by the FERM domain of Ezrin fused to GST (GST-$FERM_E$) but not with GST alone, while gD-HER2-EBM* was poorly pulled down with GST-$FERM_E$ (**Fig. 1C**), demonstrating weak binding of this mutated form to the FERM domain of ezrin.

To investigate whether this interaction was direct, we first used a protein–protein interaction assay based on oxygen singlet transfer (AlphaScreen). We detected an association between the biotinylated peptide encoding the cytosolic juxtamembrane region of HER2 (biot-JM_{HER2}) and GST-$FERM_E$, whereas a low signal was generated using GST alone or in the absence of any peptide (**Fig. 1D**). This interaction was dose-dependent (Supplementary Fig. S1B and S1C). Addition of nonbiotinylated peptide coding for the juxtamembrane region of HER2 competed with biot-JM_{HER2}/$FERM_E$ interaction in a dose-dependent manner [maximum competition effect of 80%, apparent Kd (Kda) = 13 nmol/L], whereas competition was poorly efficient upon addition of non-biotinylated HER2 peptide harboring mutations of the key residues in the EBM motif (45% inhibition, Kda = 67 nmol/L; Supplementary Fig. S1D). The biot-JM_{HER2}/$FERM_E$ interaction was in the same range of affinity as the interaction measured between GST-$FERM_E$ and a biotinylated peptide coding for the cytosolic juxtamembrane region of CD44 (biot-JM_{CD44}) containing a known ERM-binding motif (Kda = 8 nmol/L; Supplementary Fig. S1E–S1G). Second, using surface plasmon resonance (SPR), we measured a high-affinity interaction between GST-$FERM_E$ and immobilized biot-JM_{HER2} peptide (Kd = 4.49 ± 1.52 nmol/L; **Fig. 1E**), which was similar to the one observed with immobilized biot-JM_{CD44} peptide (Kd = 5.79 ± 0.12 nmol/L; Supplementary Fig. S1H). No interaction was observed with GST alone or on immobilized peptide coding for the cytosolic region of CD147 ($cyto_{CD147}$), a receptor that does not interact with ERM, as negative control (**Fig. 1E**). These results demonstrate that HER2 contains an ERM-binding motif in its cytosolic juxtamembrane region allowing direct interaction with the FERM domain of ERM proteins.

In polarized epithelial cells, such as Caco2/TC7 intestinal epithelial cells, HER2 mostly localized at the basolateral membrane (**Fig. 1F**, top), a localization resulting from the interaction of its C-terminal motif with PDZ domain–containing proteins (24, 25). A bipartite sorting signal (aa 692–701) next to the ERM-binding motif is also necessary to ensure its proper targeting to the basolateral

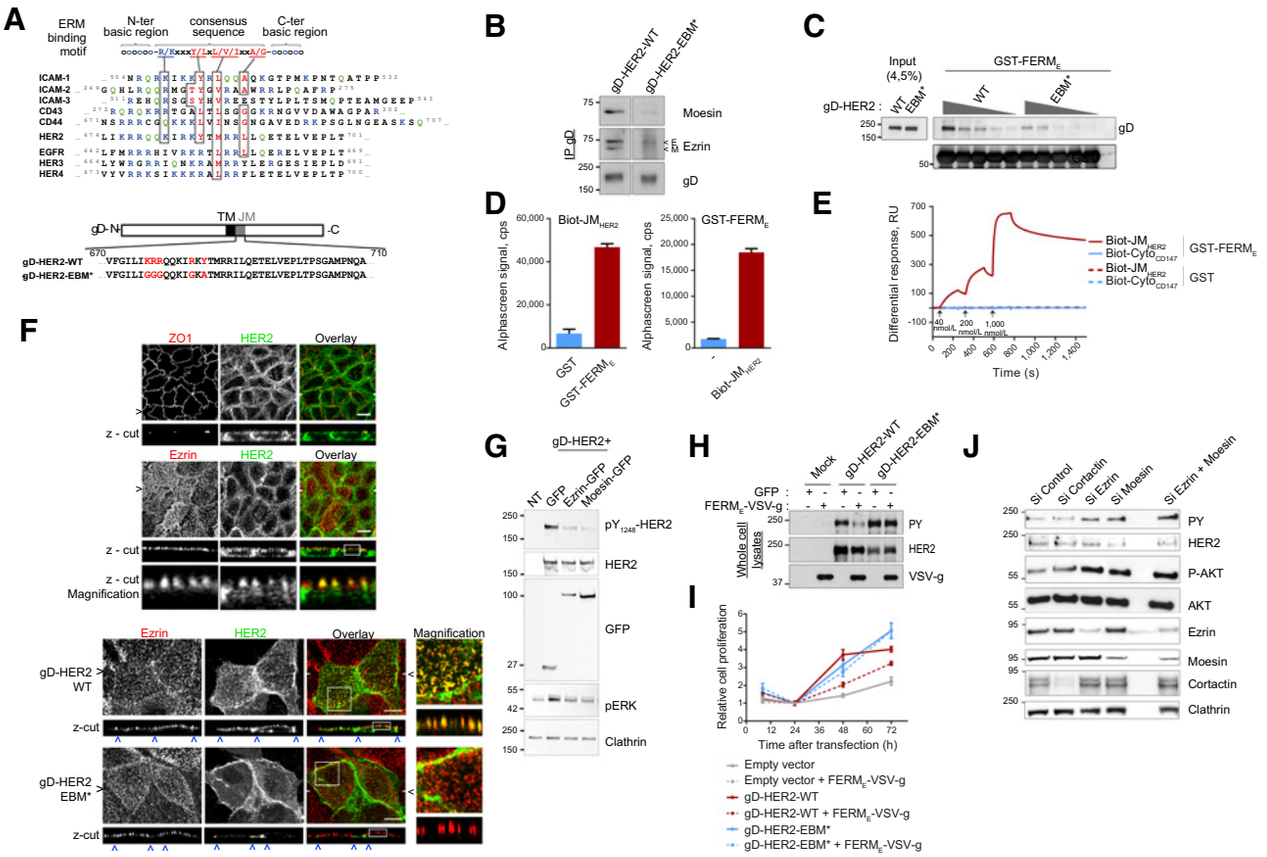

Figure 1.

HER2 interaction with the ERM proteins Ezrin and Moesin addresses HER2 in ERM-enriched regions and control its ligand-independent activation. **A,** Top, consensus sequence of the ERM-binding motif and sequence alignment of the cytoplasmic juxtamembrane regions of adhesion molecules binding ERM proteins and of the HER family members. Basic and acidic residues are shown in blue and red, respectively. The basic clusters located in the ERM-binding motif are underlined. Glutamines are shown in green. Key residues of the ICAM-2 binding motif to radixin FERM domain are boxed in brown. Bottom, schematic depiction of gD-tagged HER2 vectors showing the transmembrane domain (TM) and the juxtamembrane region (JM) of gD-tagged wild-type HER2 (gD-HER2-WT), and the mutant generated with alanine and glycine substitutions within the ERM-binding motif (gD-HER2-EBM*). **B,** HBMECs were transfected with vectors encoding gD-HER2-WT or gD-HER2-EBM*. Lysates were immunoprecipitated with an anti-gD antibody and analyzed by Western blot using anti-Moesin, anti-Ezrin, and anti-gD antibodies. **C,** Left, HBMECs were transfected with gD-HER2-WT or gD-HER2-EBM* constructs and cell lysates were analyzed by Western blot with anti-gD antibody. Right, decreasing concentrations of respective cell lysates were pulled down with GST-FERM$_E$ and analyzed by Western blot with anti-gD and anti-GST antibodies. **D,** Left, AlphaScreen assay with 125 nmol/L GST-FERM$_E$ (red), or GST (blue) incubated with 10 nmol/L biotinylated JM HER2 peptide (biot-JM$_{HER2}$). A representative experiment is shown ($n = 3$) where data are mean ± SEM ($n = 2$). Right, AlphaScreen assay with 83 nmol/L GST-FERM$_E$ incubated in the presence (red) or in the absence (blue) of 9.25 nmol/L biot-JM$_{HER2}$ peptide. Data are mean ± SEM ($n = 2$). **E,** Peptides encoding the cytosolic JM region of HER2 (biot-JM$_{HER2}$, red) or the short cytosolic tail of CD147 (cyto$_{CD147}$, blue) were captured on a streptavidin-coated sensor chip [surface immobilization level of 60 and 115 resonance units (RU), depending on their respective molecular weight]. GST (dotted lines) or GST-FERM$_E$ (solid lines) were used as analytes and injected sequentially at 40 nmol/L, 200 nmol/L, and 1,000 nmol/L to perform single-cycle kinetics. **F,** Top, confluent monolayers of Caco-2/TC7 enterocytes were labeled with anti-Z01 (red) and anti-HER2 (green) antibodies (top) or with anti-Ezrin (red) and anti-HER2 (green) antibodies (bottom). Images of xy/xz plans and xz sections (z-cut) are shown. Merged images of the same fields are presented in the right panel (overlay) and higher magnifications of the inset are presented in the bottom panels. Horizontal black arrows indicate the lines on the xy plan, where the z-cut presented underneath was selected. Bars, 10 μm. Bottom, LLC-PK1 epithelial cells transfected with vectors encoding gD-HER2-WT or gD-HER2-EBM* were labeled with anti-Ezrin (red) and anti-HER2 (green) antibodies. Images of xy/xz plans and xz sections (z-cut) are shown. Merged images of the same fields are presented in the last panel (overlay) and higher magnifications of the inset are presented in the bottom panels. Horizontal black arrows indicate the lines on the xy plan, where the z-cut presented underneath was selected, and the vertical blue arrows on the z-cuts indicate cell junctions. Bars, 10 μm. **G,** Lysates from HBMECs nontransfected (NT) or cotransfected with gD-HER2 together with GFP, Ezrin-GFP or Moesin-GFP were analyzed by Western blots using antibodies against pY1248-HER2, HER2, GFP, p-ERK, and Clathrin. **H,** Lysates from HBMECs transfected with empty vector (Mock), gD-HER2-WT, or gD-HER2-EBM* together with GFP or FERM$_E$-VSV-g were analyzed by Western blots using anti-phosphotyrosine (PY), anti-HER2, and anti-VSV-g antibodies. **I,** HBMECs were cotransfected with empty vector (Mock), gD-HER2-WT, or EBM* alone (solid lines) or together with FERM$_E$-VSV-g (dotted lines) and their proliferation was analyzed 24, 48, and 72 hours after transfection. Results are means ± SEM ($n = 4$) of a representative of three independent experiments. **J,** HBMECs were transfected with siRNA targeting Ezrin, Moesin, or cortactin or untargeted siRNA sequence as a negative control, and analyzed by Western blot using antibodies against Ezrin, Moesin, cortactin, clathrin, phosphotyrosine (PY), HER2, p-Akt, or Akt. **B–J,** Shown are representative images or Western blots of two to three independent experiments.

membrane (26). Less documented is the apical membrane localization of HER2. We observed here that HER2 localizes at the apical surface of Caco2/TC7 cells within ERM-enriched microvilli (**Fig. 1F**, top). When expressed in LLC-PK1 epithelial cells, which are deficient in the μ1B subunit of the AP1B adaptor complex, leading to significant amounts of HER2 that are missorted to the apical membrane (26), both gD-HER2 WT and gD-HER2-EBM* were found at the lateral junctions; however, only the WT form of HER2 colocalized with Ezrin within apical microvilli (**Fig. 1F**, bottom), indicating that HER2 interaction with ERM proteins controls the subcellular localization of HER2 within ERM-enriched structures.

ERM proteins control the ligand-independent activation of HER2

We next observed that, when overexpressed in HBMEC, gD-HER2-EBM* exhibited higher levels of tyrosine phosphorylation compared with gD-HER2-WT (Supplementary Fig. S2A), suggesting that loss of HER2–ERM interaction might potentiate receptor activation. To test this hypothesis, we overexpressed gD-HER2-WT in HBMEC with GFP-tagged Ezrin or Moesin. The phosphorylation level of HER2 was reduced by more than 75% when coexpressed with Ezrin or Moesin (**Fig. 1G**). Expression of Ezrin ($FERM_E$) or Moesin ($FERM_M$) FERM domains alone was sufficient to reduce the phosphorylation level of overexpressed HER2 (**Fig. 1H**; Supplementary Fig. S2B). To confirm this result, we overexpressed HER2 with VSVg-tagged Ezrin or with two previously described VSVg-tagged mutants of Ezrin: the T567D mutant mimicking the phosphorylation of a conserved threonine in the C-terminal actin-binding site, which stabilizes Ezrin in an active open conformation, and the nonphosphorylable mutant T567A (22, 27), or GFP as a negative control. The phosphorylation level of HER2 was reduced by 20% and 30% when coexpressed with Ezrin or with the T567A Ezrin mutant, and reduced by 55% when coexpressed with the T567D Ezrin mutant (Supplementary Fig. S2C). HER2 inhibition promoted by these forms of Ezrin was accompanied by a proportional reduction in the downstream activation of ERK and AKT protein kinases (**Fig. 1G**; Supplementary Fig. S2C). Accordingly, expression of gD-HER2-WT induced a 2 to 3-fold increase in the rate of endothelial cell proliferation, which was reduced by 70% to 85% when coexpressed with $FERM_E$, whereas $FERM_E$ did not affect the basal cell proliferation (**Fig. 1I**). As expected, expression of $FERM_E$ had no effect on HER2-EBM* activation (**Fig. 1H**), nor on HER2-EBM*–induced cell proliferation (**Fig. 1I**). In contrast, expression of the FERM domains of FAK or PYK2 ($FERM_F$ and $FERM_P$) had no effect despite their related structure but lesser sequence similarity (Supplementary Fig. S2B), indicating that this inhibitory effect was specific to the ERM proteins.

Conversely, depletion of Ezrin, Moesin, or both in HBMECs induced, respectively, a 2, 3, and 4-fold increase in activation of endogenous HER2, together with a 3-fold increase in AKT activation, whereas depletion of the actin-binding protein cortactin, as a control, did not affect HER2 activation (**Fig. 1J**). Accordingly, depletion of Ezrin and Moesin further increased HER2 activation and the proliferation rate of endothelial cells expressing gD-HER2-WT, while it had no further effect on HER2-EBM* activation, nor on HER2-EBM*–induced cell proliferation (Supplementary Fig. S2D and 2E). These experiments showed that Ezrin and Moesin exert a constitutive inhibitory effect that prevents the ligand-independent activation of HER2. However, although HER2 is the preferential heterodimerization partner of the other HER family members (10, 12), expression of Ezrin-VSV-g or of $FERM_E$ did not alter the ligand-dependent activation of HER2 in heterodimers with EGFR/HER1 or with HER3 upon EGF or HRG stimulation, nor downstream activation of AKT and ERK MAPK (Supplementary Fig. S2F and 2G). These results demonstrate that ERM proteins are allosteric inhibitors of HER2 by interacting with the ERM-binding motif present in its juxtamembrane region. This interaction specifically prevents the ligand-independent activation of HER2.

The unbalance in ERM/HER2 expression contributes to HER2 activation in $HER2^+$ breast cancers

Interestingly, we observed a significant inverse correlation between HER2 and Moesin transcripts [Spearman correlation coefficient (r) = −0.2866, P = 0.0161] in 70 commonly used human breast cancer cell lines, whereas a positive or no correlation between HER2 and Ezrin or Radixin mRNA expression was observed (Ezrin: $r = 0.3386$, $P = 0.0041$; Radixin: $r = -0.1509$, $P = 0.2123$; **Fig. 2A**). At the protein level, we also detected an inverse correlation between HER2 and Moesin expression in breast cancer cell lines with different HER2 status, while they expressed similar levels of Ezrin and Radixin (**Fig 2B**; Supplementary Fig. S3A and S3B). A significant inverse correlation between Moesin and HER2 mRNA expression levels ($r = -0.3010$; $P < 0.0001$) was also observed in 526 patient-derived breast-invasive carcinoma (**Fig. 2C**). Among ERM protein members, a negative correlation with HER2 expression was also seen with Radixin, whereas a positive correlation was found with Ezrin (Ezrin: $r = 0.1538$, $P = 0.0004$; Radixin: $r = -0.1783$, $P < 0.0001$; **Fig. 2C**). Likewise, IHC analysis performed on tissue microarray containing 67 ductal carcinomas with different HER2 status revealed a significant inverse correlation between Moesin and HER2 protein expression levels, while Ezrin remains expressed in $HER2^+$ breast cancers (**Fig. 2D**; Supplementary Fig. S4A–S4C). Finally, similar observation was found in most cancer types known to have abnormalities in *ERBB2* gene (cervix, stomach, bladder, pancreas, colon, ovary, and kidney; Supplementary Fig. S5). Altogether, these results indicated that low Moesin expression was significantly associated with $HER2^+$ cancers and, based on our previous results, we hypothesized that this might contribute to aberrant activation of HER2.

To test this hypothesis, we overexpressed Moesin, Ezrin, or their respective FERM domains in SKBR3 or BT474, two breast cancer cell lines overexpressing HER2 and devoid of Moesin expression (**Fig. 2B**). Their overexpression reduced the aberrant activation of HER2 by 60% in BT474 (**Fig. 2E**) and by 40% and 100%, respectively, in SKBR3 cells (Supplementary Fig. S6A). This effect was accompanied by decreased AKT activation (Supplementary Fig. S6A) and inhibition of cell proliferation (**Fig. 2F**; Supplementary Fig. S6B and S6C). Interestingly, in HCC1954 breast cancer cell line expressing Moesin, although HER2 expression level was similar to SKBR3 and BT474 cells, HER2 activation was lower in these cells (**Fig. 2B**). The overexpression of Ezrin, $FERM_E$, or Moesin in HCC1954 totally inhibited cell proliferation (Supplementary Fig. S6D and S6E). To strengthen this result, we fused $FERM_E$, or GFP as a control, to a cell-penetrating peptide derived from the Epstein–Barr virus ZEBRA transcription factor (28; Supplementary Fig. S6F). As expected, incubation of SKBR3 cells with 0.3 to 0.9 μmol/L $FERM_E$-Zebra induced a dose-dependent inhibition of HER2 activation up to 85%, whereas Zebra-GFP did not modify HER2 activation (Supplementary Fig. S6G). Altogether, these results demonstrate that ERM proteins are key allosteric regulators of HER2 activation. The unbalance in ERM/HER2 protein levels contributes to HER2 activation in $HER2^+$ breast cancers.

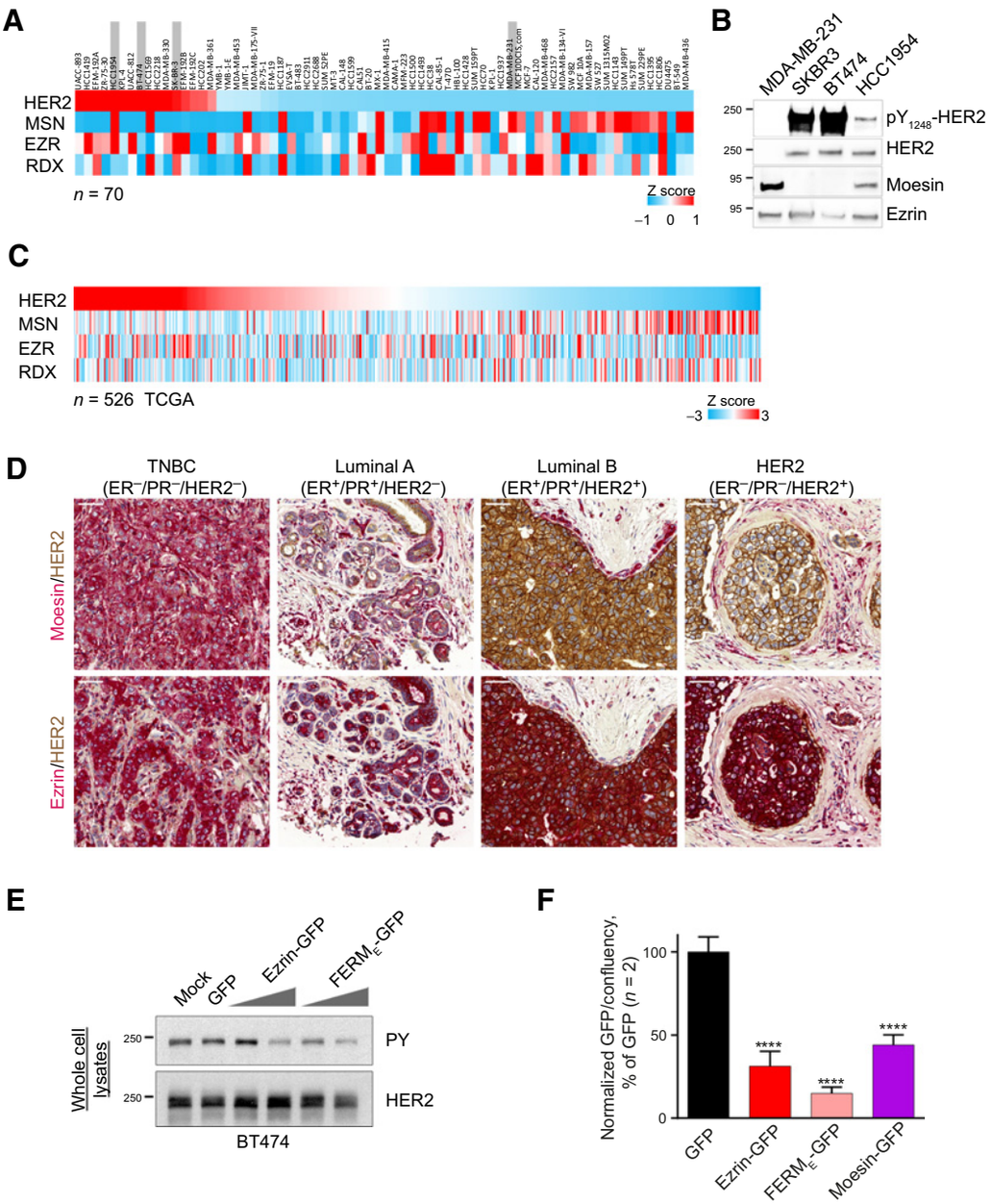

Figure 2.

The unbalance in ERM/HER2 expression contributes to HER2 activation in HER2$^+$ breast cancers. **A,** Color-coded representation of HER2, Moesin (MSN), Ezrin (EZR), or Radixin (RDX) mRNA expression levels in 70 commonly used breast cancer cell lines from E-MTAB-2706 study (https://www.ebi.ac.uk/arrayexpress/). Spearman correlation coefficients $r = -0.4771$ (MSN), $r = 0.3354$ (EZR), $r = -0.2542$ (RDX); P value (two-tailed), $P < 0.0001$ (MSN), $P = 0.0045$ (EZR), $P = 0.337$ (RDX). Cell lines used in this study are highlighted in gray. **B,** Lysates from breast cancer cell lines (MDA-MB-231, SKBR3, BT474, and HCC1954) were analyzed by Western blots using anti-phospho HER2 (pY_{1248}-HER2), anti-HER2, anti-Moesin, or anti-Ezrin antibodies. **C,** Color-coded representation of the mRNA expression level of HER2, Moesin (MSN), Ezrin (EZR), and Radixin (RDX) in samples from 526 patients with breast-invasive carcinoma from TCGA cohort (http://www.cbioportal.org). Spearman correlation coefficients $r = -0.3010$ (MSN), $r = 0.1538$ (Ezrin), $r = -0.1783$ (Radixin); P value (two-tailed) $P < 0.0001$, $P = 0.0004$ (Ezrin), $P < 0.0001$ (Radixin). **D,** Representative images of human breast carcinoma sections from each molecular subtype labeled by IHC with anti-HER2 (brown) and anti–Moesin or anti-Ezrin (red) antibodies. TNBC, triple-negative breast cancers. Bars, 50 μm. The IHC analysis performed on 67 cases of breast ductal carcinoma with known molecular subtypes is shown in Supplementary Fig. S4. **E,** Lysates of BT474 cells mock transfected, transfected with a vector encoding GFP, or with increasing concentrations of vectors encoding Ezrin-GFP or $FERM_E$-GFP, were analyzed by Western blots with anti-phosphotyrosine (PY) and anti-HER2 antibodies. Shown is a representative blot of $n = 3$ independent experiments. **F,** BT474 cells transfected with GFP, Ezrin-GFP, $FERM_E$-GFP, or Moesin-GFP were monitored by time-lapse imaging (Incucyte). Quantification of the number of GFP-positive cells over time was performed (data presented in Supplementary Fig. S6B and S6C). Shown is the quantification of GFP-positive cells ($n = 12$ fields) 72 hours posttransfection, where data are mean ± SEM ($n = 2$); one-way ANOVA followed by Bonferroni multiple comparison test. ****, $P < 0.0001$.

Identification of ERM-mimicking compounds to inhibit HER2 activation

As overexpression of ERM proteins efficiently reverted HER2 activation in $HER2^+$ breast cancers, we designed a strategy aimed at identifying ERM-mimicking compounds that would actively block HER2 (**Fig. 3A**). Compounds were first selected on their ability to interfere with the HER2/$FERM_E$ interaction measured using the above described AlphaScreen assay (**Fig. 1D**). After removal of the false positives (True hit screen), to eliminate compounds interfering with the HER2–$FERM_E$ interaction through binding to GST-$FERM_E$, we performed a counter-screening AlphaScreen assay to identify and remove hits showing competition with the CD44–$FERM_E$ interaction. The remaining hits were then characterized for their ability to directly bind to the ERM-binding motif of HER2 using SPR, to inhibit HER2 activation and HER2-dependent cell proliferation and for their absence of toxicity on cells that do not overexpress HER2. Finally, the best hits were tested *in vivo* in an orthotopic xenograft model to evaluate their ability to inhibit HER2-dependent tumor growth. 1,463 molecules were screened from two Prestwick chemical libraries consisting of small molecules composed mostly of approved drugs selected for their high chemical and pharmacologic diversity, as well as for their known bioavailability and safety in humans, and a collection of natural products, mostly derived from plants, rich in diverse chemotypes. Results of the first screen at 24 hours are shown in **Fig. 3B**. Among the 77 compounds showing inhibition of HER2–$FERM_E$ interaction, 31 were true hits confirmed in dose–response experiments (data summarized in **Table 1**). Interestingly, some compounds, such as tolfenamic acid and 4,4′-(2,3-Dimethyltetramethylene) dipyrocatechol, were already known to block the growth of $HER2^+$ cancer cells (29, 30). Eleven hits were found to selectively interfere with HER2–$FERM_E$ interaction and not with CD44–$FERM_E$ interaction, and four molecules were validated to selectively bind to the ERM-binding motif of HER2 using SPR. Among them, phenylbutazone and ebselen induced a poor inhibition of HER2 activation, isoliquiritigenin inhibited HER2 activation but, as it possessed genotoxic structural alerts, it was unsuitable for drug discovery. Finally, Zuclopenthixol hydrochloride was found to achieve potent HER2 inhibition both *in vitro* and *in vivo* (results detailed below).

Zuclopenthixol is an ERM-mimicking compound conferring efficient allosteric inhibition of HER2

In vitro, Zuclopenthixol induced a dose-dependent inhibition of the HER2–$FERM_E$ interaction reaching 87% (IC_{50} = 9.8 μmol/L) at 24 hours with no or low disruption of CD44–$FERM_E$ interaction (**Table 1**). Zuclopenthixol selectively bound to the ERM-binding motif of HER2 as assessed using SPR (Supplementary Fig. S7A) and induced a dose-dependent inhibition of gD-HER2-WT overexpressed in HBMECs, accompanied by a proportional reduction in the activation of AKT and ERK protein kinases, whereas, as expected, it had no effect on gD-HER2-EBM* activation, nor on gD-HER2-EBM*–induced activation of AKT and ERK protein kinases (Supplementary Fig S7B). Zuclopenthixol also promoted a dose-dependent inhibition of HER2 activation in SKBR3 cells (Supplementary Fig S7C). Treatment with 3–5 μmol/L Zuclopenthixol reduced by 45% and 55% the cell proliferation of SKBR3 or BT474, respectively, whereas no effect was observed on the proliferation of breast cancer cells that do no overexpress HER2 (MDA-MB-231; **Fig. 3C**; Supplementary Fig. S7D), demonstrating that this compound selectively inhibits HER2-dependent cell proliferation. Finally, as expected HCC1954 were also sensitive to the inhibitory effect of Zuclopenthixol, although they express Moesin (Supplementary Fig. S7E).

We then tested the effect of Zuclopenthixol on the anchorage-independent proliferation of breast cancer cell lines, as it correlates closely with tumorigenicity in animal model (31). Treatment with 5 μmol/L Zuclopenthixol induced a 50% decrease in the size of SKBR3 microcolonies (**Fig. 3D**) and completely blocked the development of microcolonies formed by BT474 cells (**Fig. 3E**), whereas it had no effect on the development of MDA-MB-231 microcolonies (**Fig. 3F**). As a positive control, AG1478, a nonspecific HER2 kinase inhibitor, induced a 75% decrease in the size of SKBR3 microcolonies, whereas it had no effect on the formation of MDA-MB-231 microcolonies (Supplementary Fig. S7F). These results demonstrate that Zuclopenthixol selectively inhibits the anchorage-independent proliferation of breast cancer cell lines overexpressing HER2.

Zuclopenthixol is a typical antipsychotic from the thioxanthene family (commercialized as Clopixol, Cisordinol, or Acuphase) that acts by blockade of dopamine receptors. Similar results were observed with the related thioxanthene molecule Flupenthixol (Supplementary Table S3). However, poor or no effects were observed with other closely related dopamine antagonists, such as antipsychotics of the thioxanthene family (Chlorprothixene) or phenothiazine family (Thioproperazine; Supplementary Table S3). Finally, close analogues of Zuclopenthixol were synthesized. Analogue 1 inhibited the HER2–$FERM_E$ interaction *in vitro*, HER2 activation, and the anchorage-independent growth of SKBR3, although less efficiently than Zuclopenthixol and Flupenthixol, whereas no significant effects were observed with Analogues 2 and 3 (Supplementary Table S3). These data indicate that Zuclopenthixol and Flupenthixol were the most effective compounds *in vitro*, and that they promote blockade of HER2 by a mechanism independent of their neuroleptic activity.

As expected, Zuclopenthixol also efficiently inhibited HER2 activation, as well as both the anchorage-dependent and -independent proliferation of gastric (NCI-87) and ovary (SKOV3) cell lines overexpressing HER2, demonstrating its potent action on $HER2^+$ cancers (Supplementary Fig. S8A–S8C). Finally, Zuclopenthixol induced a dose-dependent inhibition of the truncated form of HER2 (p95HER2), which is resistant to antibody-based therapy, accompanied by a reduction in activation of AKT and ERK protein kinases (Supplementary Fig. S8D), and inhibited cell proliferation induced by the expression of mutated forms of HER2, V777L and V842I, two activating mutations in the kinase domain found in patients with cancer and conferring resistance to tyrosine kinase inhibitors (Supplementary Fig. S8E). These results demonstrate that, by targeting the ERM-binding motif in the juxtamembrane region of HER2, Zuclopenthixol may confer advantages over existing HER2-targeted therapies.

Zuclopenthixol inhibits the HER2-dependent tumor growth *in vivo*

To explore the potential of Zuclopenthixol to reduce the growth of HER2-overexpressing tumors *in vivo*, we used BT474 cells orthotopically implanted in the mammary fat pad of immunodeficient NOG mice (**Fig. 4A**). Treatment with Zuclopenthixol (4 mg/kg, 5 days a week), or vehicle as a control, was initiated 19 days after cell engraftment. While control tumors followed an exponential growth curve, Zuclopenthixol treatment rapidly slowed down the tumor growth, to reach a meaningful tumor growth inhibition index of 40% 10 days posttreatment (day 29), with a sustained effect until the day 40 (**Fig. 4B** and **C**). Accordingly, tumors from Zuclopenthixol-treated mice were macroscopically smaller (**Fig. 4D**) and exhibited a 40% reduction in tumor weight compared with the control (P = 0.0196; **Fig. 4E**). Zuclopenthixol treatment was overall well tolerated as indicated with

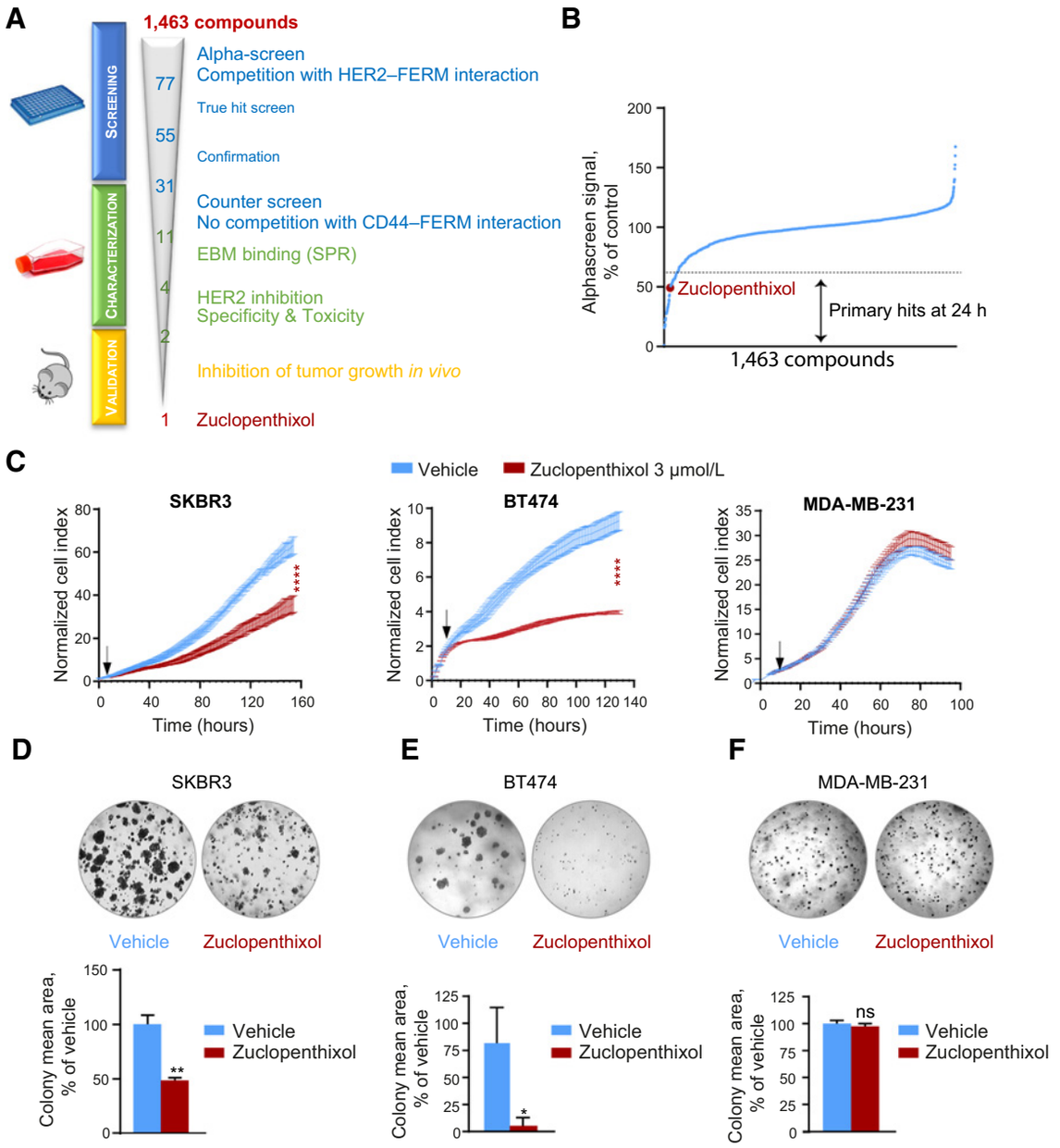

Figure 3.

Zuclopenthixol is an ERM-mimicking compound conferring allosteric inhibition of HER2. **A,** Screening strategy used to identify Moesin-mimicking compounds. A total of 1,463 drugs from commercially available libraries were screened for their ability to compete with HER2–$FERM_E$ interaction, leading to the identification of 77 first hits. After removal of the false positive, 31 remaining compounds were submitted to a counter-screen to select hits showing no competition with CD44–$FERM_E$ interaction. Eleven hits were characterized for their ability to bind peptide encoding the JM domain of HER2 in SPR, to selectively inhibit HER2 activation and HER2-dependent cell proliferation, and for their absence of toxicity on cells that do not overexpress HER2. The best hit (Zuclopenthixol) was tested *in vivo* in an orthotopic xenograft model. **B,** Signal of HER2–$FERM_E$ interaction 24 hours after the addition of compounds (Zuclopenthixol is shown in red). **C,** Proliferation curve of $HER2^+$ (SKBR3 or BT474) or HER2-negative (MDAMB-231) breast cancer cell lines treated with vehicle or with 3 µmol/L Zuclopenthixol assessed by real time impedance-based cell proliferation assay. Arrows indicate beginning of the treatment. A representative experiment is shown ($n = 2$–4) where data are mean ± SD ($n = 2$–4); statistical analysis is paired *t* test. ****, $P < 0.0001$. **D–F,** Anchorage-independent growth of SKBR3 (**D**), BT474 (**E**), or MDA-MB-231 (**F**) cells treated with vehicle or 5 µmol/L Zuclopenthixol. Representative images and quantification of the colony mean area are shown where data are mean ± SEM ($n = 2$), unpaired *t* test, **, $P < 0.01$ ($n = 5$–25; **D**); ($n = 1$), unpaired *t* test; *, $P < 0.05$ ($n = 2$–5 replicates; **F**); ($n = 1$), unpaired *t* test, ns, nonsignificant, $P = 0.59.8$ ($n = 2$–4 replicates; **F**).

Table 1. Compounds showing inhibition of HER2/FERM$_E$ interaction in AlphaScreen.

	Confirmation				Counter screen				HER2	
	Inhibition 1 h (%)	IC_{50} (μmol/L)	Inhibition 24 h (%)	IC_{50} (μmol/L)	Inhibition 1 h (%)	IC_{50} (μmol/L)	Inhibition 20 h (%)	IC_{50} (μmol/L)	interaction (SPR)	HER2 inhibition
Merbromin	98.5	0.246	86	0.46	100	0.016	ND	ND		
Chicago sky blue 6B	99	0.003	98.6	0.024	100	0.077	ND	ND		
4,4′-(2,3-Dimethyltetramethylene) dipyrocatechol	78	2.2	84	1.1	97	0.070	ND	ND		
R(-) Apomorphine hydrochloride hemihydrate	18	ND	66	3.9	35	0.16	86	9.4		
Cynarin	69	0	36	1459	96	0.055	74	0.35		
Myricetin	94	2	95	7	100	0.084	99	0.9		
Lansoprazole	49	80.9	28	22.12	83	0.007	78	22.55		
Oxybenzone	12	ND	52	1.27	0	ND	54	1.06		
Abietic Acid	64	0	0	ND	94	0.76	64	1.15		
Acitretin	82	20.1	33	23.55	87	8.95	74	11.06		
Cefsulodin sodium salt	75	1.9	29	1.559	95	4.37	69	10.3		
Ethoxyquin	85	30.5	23	21.76	82	3	68	4.92		
Tiratricol, 3,3′,5-triiodothyroacetic acid	88	6.1	89	5.4	94	0.016	ND	ND		
Alexidine dihydrochloride	65	6.2	41	157	67	4.86	29	9.50		
Carbidopa	38	0.000001	93	2.3	96	0.00005	95	36.37		
Paroxetine Hydrochloride	56	59	71	2.294	91	1.1	80	5.38		
Tenatoprazole	65	115.3	82	14.6	95	0.098	93	1.62		
Entacapone	52	0.04	42.8	0.136	68	1.18	ND	ND		
Thimerosal	53.9	0.5	20	42	94	0.0003	ND	ND		
Tolfenamic acid	62	134.5	43	26.71	65	33.68	52	26.84		
Chloroxine	64	11.7	0	ND	49	ND	0	ND	−	
Rotenone	21	0.04	61	23.8	0	N/A	0	N/A	−	
alpha-Ergocryptine	30	0.16	45	2.3	0	N/A	0	N/A	−	
Syrosingopine	37	4.6	59	7.8	0	N/A	0	N/A	−	
Bromocryptine mesylate	38	2.4	49	13.3	0	N/A	7	N/A	−	
Misoprostol	24	0.023	65	156.7	23	0.22	47	981.7	−	
Norgestimate	53	0.43	70	8.9	77	51.1	69	24.53	−	
Ebselen	77.9	0.045	39.6	43.9	52	1585	ND	ND	+	−
Phenylbutazone	60.4	0.68	16.8	667	0	ND	ND	ND	+	−
Isoliquiritigenin	33	20.3	44	4	0	N/A	15	56.7	+	+
Zuclopenthixol hydrochloride	73	50	87	9.8	0	ND	53	10.3	+	+
Total			31				11		4	2

Note: In blue are compounds that also interfere with CD44–FERM$_E$ interaction. In green are compounds that failed to interact with HER2 in SPR. In yellow are compounds that did not significantly inhibit HER2 activation. In red are compounds that selectively interfered with HER2–FERM$_E$ interaction, interacted with HER2 in SPR, and inhibited HER2 activation in HER2$^+$ breast cancer cells.
Abbreviation: N/A, not applicable; ND, not determined.

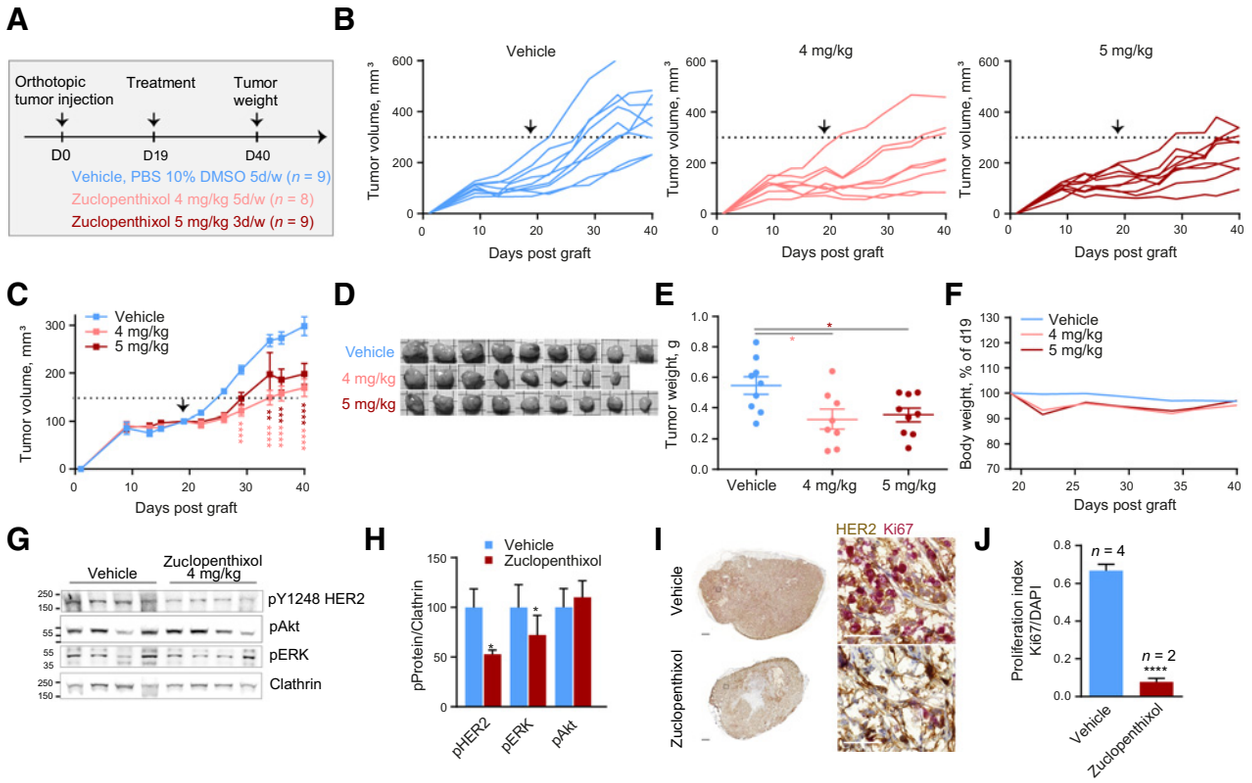

Figure 4.

Zuclopenthixol inhibits the HER2-dependent tumor growth in orthotopic xenograft model. **A–J,** 5×10^6 BT474 cells were implanted orthotopically in the mammary fat pad of NOD.Cg-Prkdc scid/J mice in the presence of estradiol supplement. After 19 days, mice were randomized in three groups ($n = 8$ or 9 mice/group) and administered intraperitoneally with Zuclopenthixol (4 mg/kg per day for 5 days a week $n = 8$, or 5 mg/kg per day for 3 days a week; $n = 9$) or vehicle (10% DMSO in PBS; $n = 9$) during 3 weeks. **A,** Scheme of the protocol used *in vivo*. **B,** Individual tumor volume of vehicle-treated or Zuclopenthixol-treated mice. Arrows indicate beginning of the treatment at day 19. **C,** Mean tumor volume of vehicle-treated or Zuclopenthixol-treated mice, normalized to the tumor volume at day 19. Data are mean ± SEM; two-way repeated-measures ANOVA followed by Bonferroni multiple comparison test. **, $P < 0.01$; ***, $P < 0.001$; ****, $P < 0.0001$. **D,** Tumors collected at the end of the experiment. **E,** Scatter plot showing tumor weight at the end of the experiment and mean ± SEM; one-way ANOVA followed by Bonferroni multiple comparison test. *, $P < 0.05$. **F,** Mean weight of mice monitored three times a week during the treatment. **G,** Western blot analysis of the tumor lysates from vehicle- or Zuclopenthixol-treated mice (4 mg/kg) using antibodies directed against activated HER2 (pY HER2), activated ERK (pERK), activated Akt (pAkt), or Clathrin as a loading control. **H,** Quantification of the results presented in **G** where data are mean ± SEM ($n = 4$), multiple paired *t* test. *, $P < 0.05$. **I,** Representative images of IHC analysis of tumor sections from vehicle- or Zuclopenthixol-treated mice using antibodies directed against HER2 (brown) and Ki67 (red). Bars, 100 μm. **J,** For quantitative analysis, sections were also labeled in immunofluorescence and the proliferation index (Ki67/DAPI) is displayed on the right where data are mean ± SEM ($n = 2$–4); unpaired *t* test. ****, $P < 0.0001$.

the monitoring of mice body weight (**Fig. 4F**). Similar results were obtained with another scheme of Zuclopenthixol administration (5 mg/kg, 3 days a week), with a tumor growth inhibition index of 30% at day 29 (**Fig. 4B** and **C**) and a 35% reduction in tumor weight compared with the control ($P = 0.0354$) (**Fig. 4C** and **D**). Biochemical analyses revealed a 45% decrease in HER2 activation in tumor lysates from Zuclopenthixol-treated animals compared to vehicle-treated animals, accompanied by a reduction in the activation of ERK protein kinases (**Fig. 4G** and **H**). In agreement with a tumor growth–inhibitory effect, Zuclopenthixol decreased by 85% the fraction of Ki67-positive tumor cells (**Fig. 4I** and **J**). Altogether, these results provide strong evidence of the potent HER2-inhibitory effect of Zuclopenthixol on human breast cancer cells overexpressing HER2 *in vivo*.

Zuclopenthixol reduces the growth of HER2-dependent brain tumors

A major issue in the management of $HER2^+$ breast cancers remains the disease progression in the central nervous system, because 30% to 50% of patients will develop brain metastases. This high incidence mainly results from the limited ability of actual therapies to cross the BBB (32) and the blood–tumor barrier remains largely intact (33). Because Zuclopenthixol is an antipsychotic with a known ability to cross the BBB, we addressed its capacity to reduce the growth of BT474 cells implanted in the caudate nucleus of the right hemisphere of immunodeficient Nude mice. Day 10 after intracranial implantation, mice were treated with Zuclopenthixol (Monday, Tuesday: 7 mg/kg; Wednesday, Thursday, Friday: 10 mg/kg; i.p.; $n = 10$) or with vehicle (i.p., $n = 10$; **Fig. 5A**). At day 20, brain tumors from the vehicle-treated group were of 75 mm^3 average size, representing a 24.3-fold increase in their growth compared with day 10. Zuclopenthixol administration was associated with smaller tumors (50 mm^3) exhibiting significantly slower progression with a 14-fold increase in their growth compared with day 10, therefore demonstrating a real benefit of Zuclopenthixol administration on $HER2^+$ brain tumor progression (**Fig. 5B–D**). We next compared the efficiency of Zuclopenthixol (Monday, Tuesday: 7 mg/kg; Wednesday, Thursday,

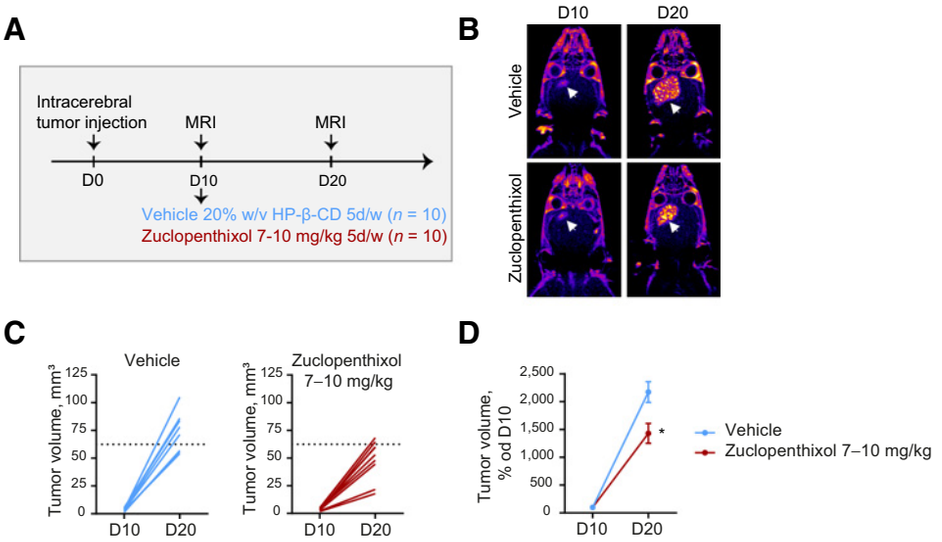

Figure 5.
Zuclopenthixol reduces the growth of HER2-dependent brain tumors. **A–D,** 1×10^5 human breast cancer BT474 cells were intracranially implanted in immunodeficient BALB/c Nude mice supplemented in estradiol. After 10 days (D10), tumor volume was evaluated by MRI and mice were randomized to be treated with Zuclopenthixol (Monday, Tuesday: 7 mg/kg; Wednesday–Friday: 10 mg/kg i.p.; $n = 10$) or with vehicle [20% w/v hydroxypropyl-β-cyclodextrin (HP-β-CD) IP; $n = 10$]. After 10 days (D20), another MRI was performed to monitor brain tumor growth. **A,** Scheme of the protocol used *in vivo*. **B,** Representative images of the MRI analysis at D10 and D20. **C,** Individual tumor volume between D10 and D20. **D,** Mean tumor volume of vehicle-treated or Zuclopenthixol-treated mice, normalized to the tumor volume at D10. Data are mean ± SEM; unpaired *t* test. *, $P = 0.0112$.

Friday: 10 mg/kg; i.p.; $n = 10$) over lapatinib (100 mg/kg 5 days/week; orally; $n = 10$; Supplementary Fig. S9A). Treatments were initiated day 3 postimplantation. At days 16 and 26, while lapatinib had no effect as compared with control mice that received vehicle, Zuclopenthixol had reduced tumor size by 35% to 50% as compared with lapatinib-treated tumors (Supplementary Fig. S9B–S9E). Combined, these data indicate that Zuclopenthixol would be promising as a therapeutic agent for $HER2^+$ breast cancer with brain metastasis.

Discussion

Much research has been conducted in recent years to improve the treatments for $HER2^+$ breast cancer, especially in light of incomplete action, adverse effects, and *de novo* or acquired resistance to HER2-targeted therapies. This implies the development of pharmaceuticals that act on mutated and truncated forms of the receptor and on brain metastatic disease, the incidence of which is increasing due to the improved management of systemic disease and increased survival rates. This study revealed an inhibitory mechanism of HER2 by the ERM proteins and the translation of this discovery into the identification of a novel class of anti-HER2 inhibitors targeting the cytosolic juxtamembrane region of HER2. Among the molecules identified, the antipsychotic drug Zuclopenthixol demonstrated a potent action on the progression of human breast cancers overexpressing HER2, on cancer cells expressing mutated or truncated forms of HER2 and, due its ability to penetrate through the BBB, on $HER2^+$ breast cancer–derived brain tumors. Overall, this inhibitor, via its mode of action, presents several advantages over existing anti-HER2 therapies and could thereby represent an important additional option in future HER2-targeted cancer therapy, in particular, for brain tumor progression.

Among the large family of RTKs, HER2 displays unusual structural features conferring unique properties. Here, we have highlighted a novel structural particularity of this receptor, which, unlike other RTK family members, possesses a functional R/KxxxYxL/V/IxxA motif allowing interaction with ERM proteins (17–19). We further demonstrated that this interaction tightly controls HER2 localization and activation. ERM proteins link membrane proteins to the cortical actin cytoskeleton, and therefore are known as key regulators of receptor localization, trafficking, and/or recycling at the cell plasma membrane thus controlling their surface availability and signaling (34). To date, direct interaction of ERM proteins with transmembrane proteins has only been described for adhesion molecules (18). The associations described between ERM proteins and several signaling receptors, including EGFR, occur indirectly through interaction with the adapter NHERF-1 (or ERM-binding phosphoprotein 50), that binds to the C-terminal sequence of these receptors (34, 35). The subcellular localization of HER2 is tightly regulated by different mechanisms, such as interaction with specific protein partners. For instance, the colocalization of HER2 with PMCA2 (plasma membrane ATPase2) in actin-rich membrane domains seems required for its stabilization at the plasma membrane (36). By interacting with NHERF-1, Ezrin may also help membrane retention of the HER2-PMCA2-NHERF-1 complex (37, 38). The interaction of the PDZ domain ERBIN to the C-terminal part of HER2 has a critical role in restricting this receptor to the basolateral membrane of epithelial cells (24). Here, we demonstrated that, by interacting directly with HER2, ERM proteins redirect HER2 receptor within ERM-rich regions. Interestingly, a basolateral targeting signal able to redirect the apically localized receptor to the basolateral membrane domain of polarized epithelial cells has also been described in the amino acid sequence following ERM-binding motif (26). Hence, our work, together with other studies, demonstrates that the cytosolic juxtamembrane region of HER2 plays a key role in the regulation of its subcellular distribution.

Previous investigations have also shown that the juxtamembrane region plays a crucial role in the activation of HER receptors upon ligand binding, by stabilizing the formation of asymmetric kinase domain dimers allowing the transphosphorylation process (39–41). Despite the unique structural conformation of the extracellular domain of HER2 locked in an open and active conformation (10), HER2 remains in inactive homodimers unless overexpressed (42), suggesting an endogenous mechanism able to restrain its ligand-independent activation (40, 41). Here, we provide evidence that interaction of ERM proteins with the juxtamembrane region of HER2

prevents this ligand-independent activation. Accordingly, loss of ERM protein expression or mutations in the ERM-binding motif of HER2 both enhanced HER2 activity. Furthermore, recurrent somatic mutations in the HER2 juxtamembrane domain were found in different patient tumors (https://cancer.sanger.ac.uk/cosmic), among which, the most frequent (R678Q) was shown to enhance HER2 activity (43). It is tempting to speculate that mutations lying in this sequence would result in HER2 activation through interference with ERM binding. Taken together, these results demonstrate that ERM proteins are key allosteric regulators of HER2 activation, most likely by exerting a constraint on the juxtamembrane region of HER2 that hampers stabilization in activated dimers. This mechanism prevents spontaneous HER2 activation in physiologic condition, suggesting that ERM binding precludes HER2-dependent oncogenic transformation, whereas loss of Moesin expression concomitant to HER2 overexpression in $HER2^+$ breast cancers further contributes to the oncogenic activation of HER2.

Interestingly, we found a highly significant inverse correlation between Moesin expression and HER2 status in both cell lines and primary tumors of different cancers, including breast, cervix, stomach, bladder, pancreas, colon, ovary, and kidney, indicating a potent role of Moesin in the development of HER2-positive cancers. As no mutation in MSN gene can account for Moesin's downregulation in HER2-positive cancers, this observation strongly suggests that epigenetic mechanisms, which perturbations represent hallmarks of human cancer cells, may directly or indirectly promote silencing of Moesin expression in HER2-positive cancer cells. Among epigenetic deregulation described in human cancers are changes in patterns of DNA methylation (44), the transcription of long noncoding RNAs, or miRNA that regulate gene expression by repressing translation and/or by promoting degradation of their target mRNA (45). Future studies will aim at characterizing the mechanisms by which Moesin expression is repressed in $HER2^+$ cancer cells.

The restriction of HER2 activation through ERM binding prompted us to translate our findings into pharmacologic intervention on $HER2^+$ breast tumors. The design of a high-throughput screening method based on this interaction to find Moesin-mimicking compounds allowed us to identify Zuclopenthixol, a neuroleptic belonging to the group of thioxanthene commonly used to treat acute episodes of mental disorders by blockade of dopamine receptors. As expected, this compound could bind the juxtamembrane region of HER2 and block HER2 activation. As a consequence, it specifically reduces HER2-dependent proliferation and $HER2^+$ breast tumor progression *in vivo*. Because of this original mode of action, Zuclopenthixol is active on several intrinsically altered forms of HER2 such as the p95-truncated form of HER2 expressed in up to 30% of patients that confers resistance to antibodies-based therapies, or oncogenic forms of HER2 with activating mutations in the kinase domain (V777L and V842I) conferring resistance to tyrosine kinase inhibitors. Finally, this compound, able to rapidly penetrate the brain, shows significant activity on the progression of aggressive $HER2^+$ breast cancer–derived brain tumors. Interestingly, the closely related dopamine antagonist Flupenthixol had similar effects, while others such as Chlorprothixene did not interact with the juxtamembrane region of HER2, demonstrating a mechanism independent of their neuroleptic activity. These effects were observed at well-tolerated doses of Zuclopenthixol hydrochloride (4–10 mg/kg in mice), higher than recommended for chronic administration in humans (150–300 mg every 2 weeks). However, concentration may be further increased by steps of 50–100 mg once or twice weekly in patients requiring higher doses, or shorter intervals between doses. In addition, the time course of the antipsychotic action revealed a progressively enhanced response to antipsychotic drugs that follows an exponential curve with repeated drug administration (46). Given these advantages over existing therapies, Zuclopenthixol or Flupenthixol, would therefore provide a valuable treatment of $HER2^+$ breast cancers and of a wide range of other HER2 overexpressing tumors, to efficiently combat primary tumors and derived brain metastases in combination with the current HER2-targeted drugs.

Taken together, through the discovery of an unexpected allosteric regulation of HER2 activation by the ERM proteins, we identified Zuclopenthixol as an ERM-mimicking compound. Our work reveals a new approach to target oncogenic forms of HER2. It provides the proof of concept that Zuclopenthixol possesses efficient antitumor activity in $HER2^+$ primary cancers and brain metastases and could be used in addition to HER2-targeted therapies to prevent and treat $HER2^+$ cancers.

Authors' Disclosures

C. Faure, A. Domingot, and S. Bourdoulous report a patent for Diagnosis and/or Prognosis of HER2-Dependent Cancer using Moesin as a Biomarker, WO/2019/081608, pending. J. Lenormand reports grants from Linksium during the conduct of the study; grants from ANR; and grants from Linksium outside the submitted work; in addition, J. Lenormand has a patent for WO2011135222 (A3) issued. No disclosures were reported by the other authors.

Authors' Contributions

C. Faure: Conceptualization, formal analysis, funding acquisition, investigation, writing–original draft, writing–review and editing. **R. Djerbi-Bouillié:** Conceptualization, formal analysis, investigation. **A. Domingot:** Investigation. **H. Bouzinba-Segard:** Investigation. **S. Taouji:** Methodology. **Y. Saidi:** Investigation. **S. Bernard:** Investigation. **F. Carallis:** Investigation. **R. Rothe-Walther:** Methodology. **J. Lenormand:** Validation, investigation. **E. Chevet:** Conceptualization, validation. **S. Bourdoulous:** Conceptualization, formal analysis, supervision, funding acquisition, validation, writing–original draft, writing–review and editing.

Acknowledgments

The authors thank B.B. Weksler, M. Rousset, M. Arpin, J. Delon, J. Baselga, M. Sliwkowski, H. Enslen, and E Charafe-Jauffret for kindly providing reagents. They thank Remy Castellano and Yves Collette of the TrGET platform (Institut Paoli Calmettes) and Oncodesign for the animal experiments. The authors thank the Biophysical and Structural Chemistry platform of the Institut Européen de Chimie et Biologie (Pessac/Bordeaux, France) and the platforms of the Institut Cochin (Imag'IC, Cybio, HistIM) for their expert technical assistance. This work was supported by the Centre National de la Recherche Scientifique, the Institut National de la Santé et de la Recherche Médicale, the Université de Paris, the Association pour la Recherche contre le Cancer (SFI20101201780 and PJA 20131200363), The Fondation de France (00016391), the GEFLUC Association (GEFLUC2016), and the Société de Transfert de Technologies (SATT) Ile de France Innov (ANR-10-SATT-05-01). C. Faure was supported by Fondation de France and SATT. R. Djerbi-Bouillié was supported by a doctoral fellowship from the Ministère de la Recherche and by ARC. A. Domingot was supported by a doctoral fellowship from the Ligue Contre le Cancer and ARC. S. Bernard was supported by a doctoral fellowship from the Université Paris Diderot and ARC.

The costs of publication of this article were defrayed in part by the payment of page charges. This article must therefore be hereby marked *advertisement* in accordance with 18 U.S.C. Section 1734 solely to indicate this fact.

Received January 15, 2021; revised July 27, 2021; accepted September 2, 2021; published first September 7, 2021.

References

1. Du Z, Lovly CM. Mechanisms of receptor tyrosine kinase activation in cancer. Mol Cancer 2018;17:58.
2. Montor WR, Salas A, Melo FHM. Receptor tyrosine kinases and downstream pathways as druggable targets for cancer treatment: the current arsenal of inhibitors. Mol Cancer 2018;17:55.
3. Kreutzfeldt J, Rozeboom B, Dey N, De P. The trastuzumab era: current and upcoming targeted HER2+ breast cancer therapies. American journal of cancer research 2020;10:1045–67.
4. Saez R, Molina MA, Ramsey EE, Rojo F, Keenan EJ, Albanell J, et al. p95HER-2 predicts worse outcome in patients with HER-2-positive breast cancer. Clin Cancer Res 2006;12:424–31.
5. Chumsri S, Sperinde J, Liu H, Gligorov J, Spano JP, Antoine M, et al. High p95HER2/HER2 ratio associated with poor outcome in trastuzumab-treated HER2-positive metastatic breast cancer NCCTG N0337 and NCCTG 98–32–52 (Alliance). Clin Cancer Res 2018;24:3053–8.
6. Connell CM, Doherty GJ. Activating HER2 mutations as emerging targets in multiple solid cancers. ESMO open 2017;2:e000279.
7. Kodack DP, Askoxylakis V, Ferraro GB, Fukumura D, Jain RK. Emerging strategies for treating brain metastases from breast cancer. Cancer Cell 2015; 27:163–75.
8. Ullrich A, Schlessinger J. Signal transduction by receptors with tyrosine kinase activity. Cell 1990;61:203–12.
9. Olayioye MA, Neve RM, Lane HA, Hynes NE. The ErbB signaling network: receptor heterodimerization in development and cancer. EMBO J 2000;19: 3159–67.
10. Garrett TP, McKern NM, Lou M, Elleman TC, Adams TE, Lovrecz GO, et al. The crystal structure of a truncated ErbB2 ectodomain reveals an active conformation, poised to interact with other ErbB receptors. Mol Cell 2003;11:495–505.
11. Di Fiore PP, Pierce JH, Kraus MH, Segatto O, King CR, Aaronson SA. erbB-2 is a potent oncogene when overexpressed in NIH/3T3 cells. Science 1987;237: 178–82.
12. Graus-Porta D, Beerli RR, Daly JM, Hynes NE. ErbB-2, the preferred heterodimerization partner of all ErbB receptors, is a mediator of lateral signaling. EMBO J 1997;16:1647–55.
13. She QB, Chandarlapaty S, Ye Q, Lobo J, Haskell KM, Leander KR, et al. Breast tumor cells with PI3K mutation or HER2 amplification are selectively addicted to Akt signaling. PLoS One 2008;3:e3065.
14. Junttila TT, Akita RW, Parsons K, Fields C, Phillips GDL, Friedman LS, et al. Ligand-independent HER2/HER3/PI3K complex is disrupted by trastuzumab and is effectively inhibited by the PI3K inhibitor GDC-0941. Cancer Cell 2009; 15:429–40.
15. Hughes SC, Fehon RG. Understanding ERM proteins–the awesome power of genetics finally brought to bear. Curr Opin Cell Biol 2007;19:51–6.
16. Bretscher A, Edwards K, Fehon RG. ERM proteins and merlin: integrators at the cell cortex. Nat Rev Mol Cell Biol 2002;3:586–99.
17. Yonemura S, Hirao M, Doi Y, Takahashi N, Kondo T, Tsukita S. Ezrin/radixin/moesin (ERM) proteins bind to a positively charged amino acid cluster in the juxta-membrane cytoplasmic domain of CD44, CD43, and ICAM-2. J Cell Biol 1998;140:885–95.
18. Hamada K, Shimizu T, Yonemura S, Tsukita S, Hakoshima T. Structural basis of adhesion-molecule recognition by ERM proteins revealed by the crystal structure of the radixin-ICAM-2 complex. Embo J 2003;22:502–14.
19. Mori T, Kitano K, Terawaki S, Maesaki R, Fukami Y, Hakoshima T. Structural basis for CD44 recognition by ERM proteins. J Biol Chem 2008;283:29602–12.
20. Schweitzer KM, Vicart P, Delouis C, Paulin D, Drager AM, Langenhuijsen MM, et al. Characterization of a newly established human bone marrow endothelial cell line: distinct adhesive properties for hematopoietic progenitors compared with human umbilical vein endothelial cells. Lab Invest 1997;76:25–36.
21. Chantret I, Rodolosse A, Barbat A, Dussaulx E, Brot-Laroche E, Zweibaum A, et al. Differential expression of sucrase-isomaltase in clones isolated from early and late passages of the cell line Caco-2: evidence for glucose-dependent negative regulation. J Cell Sci 1994;107:213–25.
22. Gautreau A, Louvard D, Arpin M. Morphogenic effects of ezrin require a phosphorylation-induced transition from oligomers to monomers at the plasma membrane. J Cell Biol 2000;150:193–203.
23. Lambotin M, Hoffmann I, Laran-Chich MP, Nassif X, Couraud PO, Bourdoulous S. Invasion of endothelial cells by Neisseria meningitidis requires cortactin recruitment by a phosphoinositide-3-kinase/Rac1 signalling pathway triggered by the lipo-oligosaccharide. J Cell Sci 2005;118: 3805–16.
24. Borg JP, Marchetto S, Le Bivic A, Ollendorff V, Jaulin-Bastard F, Saito H, et al. ERBIN: a basolateral PDZ protein that interacts with the mammalian ERBB2/HER2 receptor. Nat Cell Biol 2000;2:407–14.
25. Shelly M, Mosesson Y, Citri A, Lavi S, Zwang Y, Melamed-Book N, et al. Polar expression of ErbB-2/HER2 in epithelia. Bimodal regulation by Lin-7. Dev Cell 2003;5:475–86.
26. Dillon C, Creer A, Kerr K, Kumin A, Dickson C. Basolateral targeting of ERBB2 is dependent on a novel bipartite juxtamembrane sorting signal but independent of the C-terminal ERBIN-binding domain. Mol Cell Biol 2002;22:6553–63.
27. Fievet BT, Gautreau A, Roy C, Del Maestro L, Mangeat P, Louvard D, et al. Phosphoinositide binding and phosphorylation act sequentially in the activation mechanism of ezrin. J Cell Biol 2004;164:653–9.
28. Rothe R, Liguori L, Villegas-Mendez A, Marques B, Grunwald D, Drouet E, et al. Characterization of the cell-penetrating properties of the Epstein-Barr virus ZEBRA trans-activator. J Biol Chem 2010;285:20224–33.
29. Liu X, Abdelrahim M, Abudayyeh A, Lei P, Safe S. The nonsteroidal anti-inflammatory drug tolfenamic acid inhibits BT474 and SKBR3 breast cancer cell and tumor growth by repressing erbB2 expression. Mol Cancer Ther 2009;8: 1207–17.
30. Zavodovskaya M, Campbell MJ, Maddux BA, Shiry L, Allan G, Hodges L, et al. Nordihydroguaiaretic acid (NDGA), an inhibitor of the HER2 and IGF-1 receptor tyrosine kinases, blocks the growth of HER2-overexpressing human breast cancer cells. J Cell Biochem 2008;103:624–35.
31. Schwartz MA. Integrins, oncogenes, and anchorage independence. J Cell Biol 1997;139:575–8.
32. Witzel I, Oliveira-Ferrer L, Pantel K, Muller V, Wikman H. Breast cancer brain metastases: biology and new clinical perspectives. Breast Cancer Res 2016;18:8.
33. Tanaka Y, Hirata M, Shinonome S, Torii M, Nezasa KI, Tanaka H. Distribution analysis of epertinib in brain metastasis of HER2-positive breast cancer by imaging mass spectrometry and prospect for antitumor activity. Sci Rep 2018;8:343.
34. McClatchey AI, Fehon RG. Merlin and the ERM proteins–regulators of receptor distribution and signaling at the cell cortex. Trends Cell Biol 2009;19:198–206.
35. Weinman EJ, Hall RA, Friedman PA, Liu-Chen LY, Shenolikar S. The association of NHERF adaptor proteins with g protein-coupled receptors and receptor tyrosine kinases. Annu Rev Physiol 2006;68:491–505.
36. Jeong J, VanHouten JN, Dann P, Kim W, Sullivan C, Yu H, et al. PMCA2 regulates HER2 protein kinase localization and signaling and promotes HER2-mediated breast cancer. Proc Natl Acad Sci U S A 2016;113:E282–90.
37. Jeong J, Choi J, Kim W, Dann P, Takyar F, Gefter JV, et al. Inhibition of ezrin causes PKCalpha-mediated internalization of erbb2/HER2 tyrosine kinase in breast cancer cells. J Biol Chem 2019;294:887–901.
38. Jeong J, VanHouten JN, Kim W, Dann P, Sullivan C, Choi J, et al. The scaffolding protein NHERF1 regulates the stability and activity of the tyrosine kinase HER2. J Biol Chem 2017;292:6555–68.
39. Zhang X, Gureasko J, Shen K, Cole PA, Kuriyan J. An allosteric mechanism for activation of the kinase domain of epidermal growth factor receptor. Cell 2006; 125:1137–49.
40. Jura N, Endres NF, Engel K, Deindl S, Das R, Lamers MH, et al. Mechanism for activation of the EGF receptor catalytic domain by the juxtamembrane segment. Cell 2009;137:1293–307.
41. Brewer MR, Choi SH, Alvarado D, Moravcevic K, Pozzi A, Lemmon MA, et al. The juxtamembrane region of the EGF receptor functions as an activation domain. Mol Cell 2009;34:641–51.
42. Nagy P, Claus J, Jovin TM, Arndt-Jovin DJ. Distribution of resting and ligand-bound ErbB1 and ErbB2 receptor tyrosine kinases in living cells using number and brightness analysis. Proc Natl Acad Sci U S A 2010;107:16524–9.
43. Pahuja KB, Nguyen TT, Jaiswal BS, Prabhash K, Thaker TM, Senger K, et al. Actionable activating oncogenic ERBB2/HER2 transmembrane and juxtamembrane domain mutations. Cancer Cell 2018;34:792–806.
44. You JS, Jones PA. Cancer genetics and epigenetics: two sides of the same coin? Cancer Cell 2012;22:9–20.
45. He L, Hannon GJ. MicroRNAs: small RNAs with a big role in gene regulation. Nat Rev Genet 2004;5:522–31.
46. Li M. Antipsychotic-induced sensitization and tolerance: Behavioral characteristics, developmental impacts, and neurobiological mechanisms. J Psychopharmacol 2016;30:749–70.